Conversion of biomass-derived ethyl levulinate into γ-valerolactone via hydrogen transfer from supercritical ethanol over a ZrO2 catalyst

ARTICLE *in* RSC ADVANCES · JUNE 2013

Impact Factor: 3.71 · DOI: 10.1039/C3RA41288A

6 AUTHORS, INCLUDING:

Xing Tang ()
Xiamen University
16 PUBLICATIONS **91** CITATIONS
SEE PROFILE

Lei Hu
Huaiyin Normal University
24 PUBLICATIONS **132** CITATIONS
SEE PROFILE

Yong Sun
Xiamen University
35 PUBLICATIONS **246** CITATIONS
SEE PROFILE

RSC Advances

RSC Publishing

PAPER

View Article Online
View Journal | View Issue

Cite this: *RSC Advances*, 2013, **3**, 10277

Conversion of biomass-derived ethyl levulinate into γ-valerolactone *via* hydrogen transfer from supercritical ethanol over a ZrO_2 catalyst†

Xing Tang, Lei Hu, Yong Sun,* Geng Zhao, Weiwei Hao and Lu Lin*

Received 7th January 2013,
Accepted 10th April 2013

DOI: 10.1039/c3ra41288a

www.rsc.org/advances

A green and efficient process was developed for the conversion of biomass-derived ethyl levulinate (EL) into γ-valerolactone (GVL) using supercritical ethanol as the hydrogen donor and the reaction medium over low-cost and eco-friendly ZrO_2 catalysts, which were prepared by the precipitation method and characterized by BET, SEM, XRD, FT-IR, TGA-DTA, TPD-NH_3 and TPD-CO_2. The results indicated that amorphous ZrO_2 with a high specific surface area and a large number of acid–base sites exhibited the highest catalytic activity, an excellent GVL yield of 81.5% with 95.5% EL conversion was achieved at 523 K over 3 h. In addition, combined with the results of poisoning experiments, a plausible mechanism of catalytic transfer hydrogenation (CTH) *via* a six-membered ring transition state was also presented.

Introduction

With the gradual depletion of fossil resources and the continued deterioration of environmental quality, the search for renewable resources is critically important. Among the various renewable resources, biomass, which is widespread, abundant and inexpensive, is regarded as an excellent substitute for nonrenewable fossil resources. In recent years, a promising approach for the utilization of biomass has been to produce various chemicals.[1–6] Among these chemicals, GVL, which is identified as a versatile intermediate for the production of high value-added chemicals and high performance liquid fuels (Scheme 1), has attracted worldwide attention.[7–15]

In a considerable number of studies in this field, GVL is obtained by the hydrogenation of levulinic acid (LA), a precursor that can be derived from the hydrolysis of various carbohydrates such as glucose, fructose, sucrose, or cellulose. Generally, the hydrogenation of LA is driven by external molecular H_2 over noble metal catalysts (such as Rh, Pt, Ru, Ir).[16–26] In addition, the hydrogenation of LA can also be driven by internal molecular H_2 derived from the decomposition of formic acid (FA) over supported gold catalysts or immobilized Ru catalysts.[27–30] Although good yields of GVL were obtained, these catalysts used for the hydrogenation of LA or the decomposition of FA are very expensive and easily deactivated. Moreover, LA and FA are very corrosive, which will inevitably increase production costs in prospective applications. Furthermore, the production of LA is an energy-intensive process due to its high boiling point. Taking the above-mentioned problems into consideration, development of a green and low-cost approach for the synthesis of GVL is urgently needed.

In contrast to LA, the low boiling point, acid-free and easily-separable EL, produced by the ethanolysis of various carbohydrates such as glucose, fructose, sucrose, or cellulose, is a better alternative for the synthesis of GVL.[31] Recently, Zhao *et al.*[32] demonstrated a high-pressure direct liquefaction process through supercritical ethanolysis over metal oxides, GVL was detected in the mixture after reaction. Dumesic *et al.* reported the catalytic transfer hydrogenation (CTH) of LA and its esters into GVL through the Meerwein–Ponndorf–Verley (MPV) reaction over metal oxide catalysts using alcohols as the hydrogen donors in the presence of an alkylphenol.[33] However, the elevated additional pressure with He (300 psi) and the prolonged reaction time (8–16 h) were prerequisite for ensuring a high yield of GVL. Moreover, the introduction of alkylphenol will complicate the subsequent separation step of GVL.

Herein, the conversion of EL into GVL *via* CTH in supercritical ethanol without any external gas was reported. A series of low-cost and environmentally benign ZrO_2 catalysts was prepared and characterized, and various reaction parameters were investigated in order to obtain a higher yield of GVL.

School of Energy Research, Xiamen University, Xiamen 361005, China. E-mail: sunyong@xmu.edu.cn; lulin@xmu.edu.cn; Fax: +86-0592-5952786; Tel: +86-0592-5952786

† Electronic supplementary information (ESI) available. See DOI: 10.1039/c3ra41288a

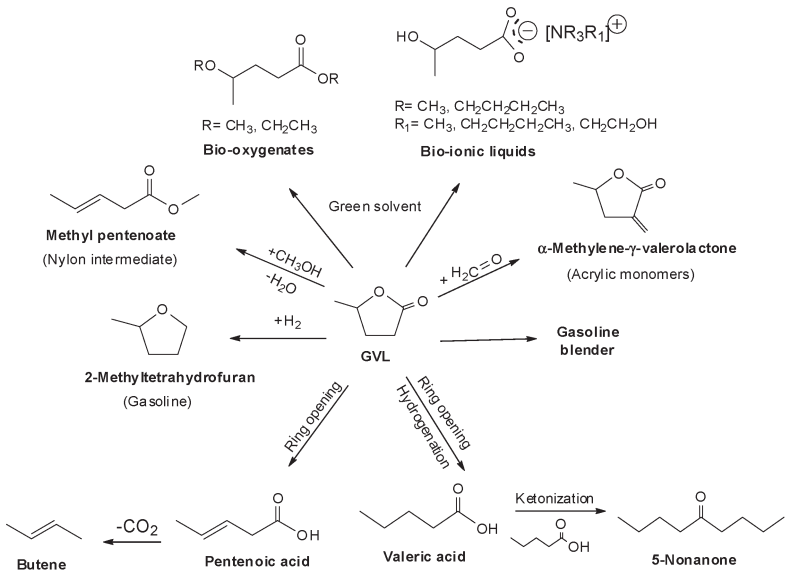

Scheme 1 The pathway for the conversion of GVL into chemicals and fuels.

Results and discussion

In order to study the catalysis of ZrO_2 solids during the CTH of EL, the detailed characterization of the ZrO_2 catalysts obtained at different calcination temperatures was carried out.

XRD patterns and the textural properties of ZrO_2 catalysts are given in Fig. 1 and Table 1, respectively. It can be seen that ZrO_2-573 and ZrO_2-773 existed as an amorphous phase and as a mixture of a monoclinic phase and a tetragonal phase, respectively, which is confirmed from the results of Djurado *et al.*[34] and Kanade *et al.*[35] When the calcination temperature was further increased to 973 K, only a monoclinic phase is present in the ZrO_2 catalyst and its diffraction peaks become more intense and sharp. Elevated temperatures facilitate the growth and perfection of ZrO_2 crystals, which correspondingly results in the increase of the particle sizes and the decrease of the specific surface areas (Table 1).

The CO_2-TPD and NH_3-TPD measurements were performed to characterize the acid–base properties of the catalyst, the results are presented in Fig. 2 and 3, respectively.

The CO_2-TPD profile of ZrO_2-573 exhibits a significant desorption peak at 416 K and a small desorption peak at 650 K, which can be assigned to the medium basic sites and the strong basic sites where CO_2 is adsorbed in the form of bidentate carbonate and unidentate carbonate, respectively (Scheme 2), and these results are in line with the study of Urbano *et al.*[36] Moreover, it is obvious that medium basic sites are dominant in ZrO_2-573. Compared to ZrO_2-573, there are fewer medium basic sites on the surface of ZrO_2-773, and no evident desorption peak is observed in the CO_2-TPD profile of ZrO_2-973. Similarly, a broad NH_3 desorption peak that can be assigned to the medium acidic sites is observed at around 545 K in the NH_3-TPD profile of ZrO_2-573, and NH_3 desorption peaks in the profiles of ZrO_2-773 and ZrO_2-973 are not apparent.

In the profiles of TPD, the number of acid–base sites is reflected by the peak areas. As can be seen from Fig. 2 and 3,

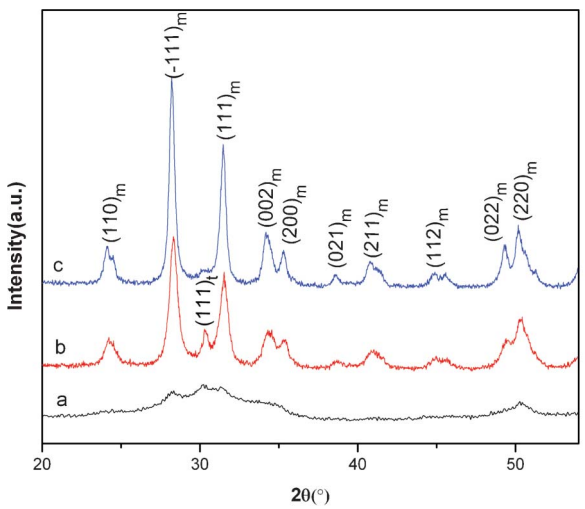

Fig. 1 XRD patterns for (a) ZrO_2-573; (b) ZrO_2-773; (c) ZrO_2-973; m = monoclinic phase; t = tetragonal phase.

Table 1 Specific surface area and textural properties of ZrO_2 obtained at different calcination temperatures

Solid	S_{BET}[a] ($m^2\ g^{-1}$)	Particle size[b] (nm)	Crystallinity[b] (%)
ZrO_2-573	157.2	Amorphous	Amorphous
ZrO_2-773	40.6	12	72.3
ZrO_2-973	27.3	23	97.7

[a] Determined by BET analysis of N_2 adsorption isotherms. [b] As XRD determined, where m = monoclinic phase; t = tetragonal phase.

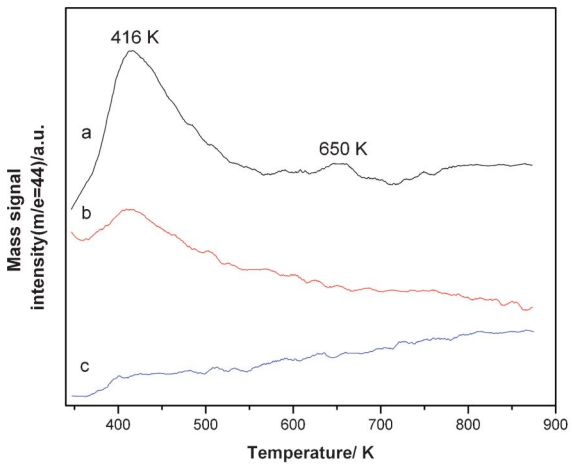

Fig. 2 CO_2-TPD profiles for (a) ZrO_2-573, (b) ZrO_2-773 and (c) ZrO_2-973.

there are many more acidic sites and basic sites in ZrO_2-573 than in ZrO_2-773 and ZrO_2-973, respectively, which may be attributed to the lower specific surface areas of ZrO_2 calcined at 773 and 973 K leading to fewer acid–base sites.

The results from FT-IR spectroscopy of ZrO_2 catalysts are shown in Fig. 4. The broad band at 3400–3500 cm^{-1} is due to the stretching vibration of the hydroxyl. The peak at 742 cm^{-1} is representative of monoclinic zirconia.[35] The band at 1621 cm^{-1} is assigned to O–C–O stretching modes of CO_2 absorbed from the atmosphere. The band at 1330 cm^{-1} is attributed to bidentate carbonates (Scheme 2).[37] However, no obvious peak is observed at 1330 cm^{-1} in the FT-IR spectrum of ZrO_2-973, which may be ascribed to ZrO_2-973 having no obvious acid–base sites.

In addition, the thermogravimetric analysis of the catalysts was conducted and the results are given in Fig. S1 and S2, ESI.† In contrast to ZrO_2-773 and ZrO_2-973, a significant mass loss (about 4 wt%) occurred when the ZrO_2-573 was heated from 293 to 373 K. This can be assigned to the loss of physically

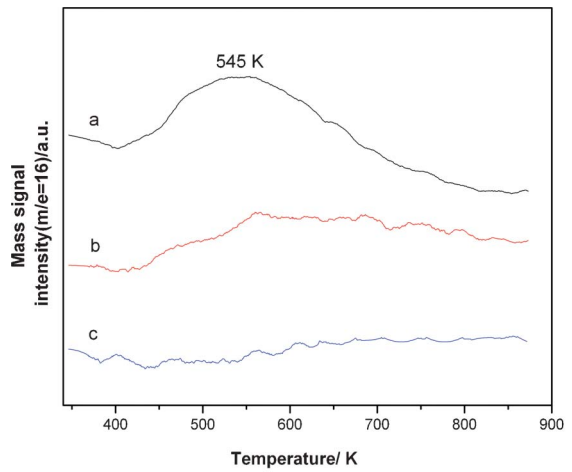

Fig. 3 NH_3-TPD profiles for (a) ZrO_2-573, (b) ZrO_2-773 and (c) ZrO_2-973.

adsorbed water, and indicated that ZrO_2-573 with a high specific area can adsorb much water. Moreover, the mass drop of ZrO_2-573 occurred continuously with increasing temperature after 373 K, and a sharp exothermic peak appeared at around 725 K (Fig. S2, ESI†). The exothermic event is attributed to a release of the hydroxyl groups of the remaining Zr-OH species in the incomplete ZrO_2 lattice, resulting in the formation and crystallization of the amorphous zirconia.[37] Furthermore, the mass loss of ZrO_2-573 did not exceed 4 wt% when the temperature was increased beyond 373 K, which indicated that only a small percentage of defective ZrO_2 lattice existed in ZrO_2-573. In conclusion, the OH bands in the FT-IR spectrum were a result of both remaining Zr-OH species and water adsorbed on the surface of the catalyst.

SEM images show that both fresh and spent ZrO_2 catalysts consisted of primary crystallites (Fig. 5). Most of these primary crystallites are smaller than 10 nm in ZrO_2-573 (Fig. 5(a)), indicating ZrO_2-573 has a large specific surface area, which is in agreement with the results in Table 1. However, the diameter of primary crystallites increased to 30–40 nm and 50–100 nm in ZrO_2-773 and ZrO_2-973, respectively. In line with the results of the XRD, the SEM images also indicate that the crystallites become bigger and bigger with an increase in calcination temperature. Moreover, the size of the primary crystallites and the surface morphology of the catalysts were apparently not changed before and after use.

Given the wide differences in the results of the catalyst characterizations, the CTH of EL was performed over various catalysts in supercritical ethanol (Table 2, entries 8, 11 and 12).

ZrO_2-573 was the most active. Compared with ZrO_2-573, the catalytic activities of ZrO_2-773 and ZrO_2-973 were very poor, leading to less than 30% GVL yield and 35% EL conversion, respectively, which is probably due to there being fewer acid–base sites on their surface.

Then, based on the good performance of the amorphous ZrO_2, the conversion of EL into GVL was conducted in the presence of ethanol using ZrO_2-573 as the catalyst (Table 2). When the reaction temperature was 453 K, only a 23.4% GVL yield and a 35.9% EL conversion were achieved. When the reaction temperature was elevated to 523 K, the reaction pressure approached 70 bar, which is in the supercritical state of ethanol (T_c = 516.2 K, P_c = 63.8 bar). Under the present conditions, a 62.5% yield of GVL and an 81.5% conversion of EL were obtained. Moreover, 43.0% GVL yield and 55.6% EL conversion were still achieved when the substrate concentration was increased to 10 wt% (Table 2, entry 9). When the reaction temperature was further increased to 533 K, EL conversion was correspondingly improved to 83.7%, however, the GVL yield dropped down to 60.8%, indicating that more byproducts were formed due to the extra-high reaction temperature. Therefore, moderate reaction temperature of 523 K was chosen for the conversion of EL into GVL in the subsequent experiments. Besides ethanol, other alcohols were also used as the hydrogen donor for the reduction of EL (Table S1, ESI†). The corresponding levulinates, other than EL, formed by transesterification when another alcohol replaced

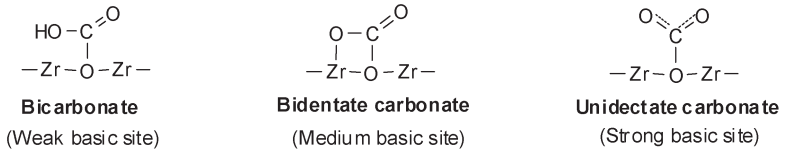

Scheme 2 Three types of interactions of CO_2 with basic sites on the surface of ZrO_2.

ethanol as the solvent and the catalysts seem to become more active in isopropanol and 1-butanol media.

In addition, it should be pointed out that ethanol as a hydrogen donor is much cheaper and safer than H_2. Meanwhile, the unreacted ethanol can be easily recovered and reused. Another advantage of CTH in the presence of ethanol is that the pressure spontaneously caused by the swelling of ethanol under elevated temperature is sufficient to maintain the supercritical state of ethanol. Hence, no additional gas needs to be introduced into the reaction system.

The EL conversion was also strongly related to the reaction time. As illustrated in Fig. 6, a yield of only 28.0% GVL and a 39.1% EL conversion were obtained after 0.5 h. The yield of GVL was further increased and then fell when the reaction time was increased from 1 to 4 h, however, EL conversion was enhanced continuously, which indicates that more and more undesired reactions, such as aldol condensation between EL, GVL and aldehydes (derived from the dehydrogenation of ethanol) occurred when the reaction time exceeded 3 h, leading to a decrease in the yield of GVL.

The effects of the dosage of the catalyst on the conversion of EL into GVL are given in Table 3. In the absence of ZrO_2-573, the GVL yield is negligible. When 0.3 g ZrO_2-573 was used, a GVL yield of 37.7% and a 46.0% conversion of EL were observed. Increasing the amount of ZrO_2-573 from 0.5 to 1 g resulted in a remarkable increase in the yield of GVL, from 46.2 to 62.5%, and the conversion of EL from 54.6 to 81.5%, respectively. When the amount of ZrO_2-573 was further increased to 1.2 g, only slight increases in the GVL yield and the EL conversion were observed. From the viewpoint of economy, the amount of 1 g was selected as an appropriate catalyst loading.

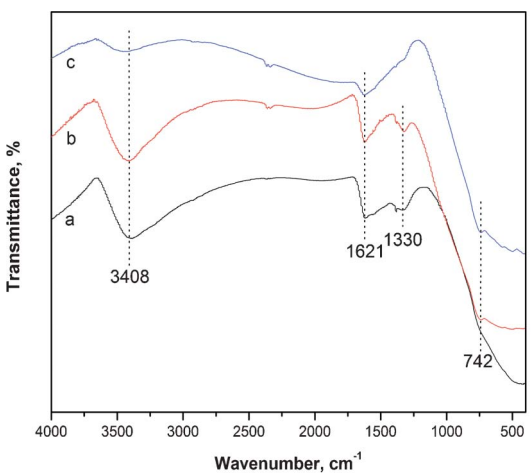

Fig. 4 FT-IR patterns for (a) ZrO_2-573, (b) ZrO_2-773 and (c) ZrO_2-973.

The long-term stability and reusability of the catalyst are extremely important considerations for the practical conversion of EL into GVL to reduce the manufacturing cost. Therefore, in this work, the recyclability of ZrO_2-573 was tested. After the first reaction cycle, ZrO_2-573 was separated from the reaction mixture by filtration without any other further treatment, and then reused in the next cycle under the same reaction conditions. As can be seen from Fig. 7, an evident decrease in the EL conversion from 81.5 to 64.9% and GVL yield from 62.5 to 50.1% was observed in the second cycle. The conversion of EL and the yield of GVL gradually dropped down to 54.6 and 43.3% when ZrO_2-573 was used 4 times, respectively. The decrease was possibly due to the partial deactivation of ZrO_2-573 caused by the deposition of humins (probably formed by an aldol condensation between EL, GVL and an aldehyde) on the surface of ZrO_2-573.

Fortunately, the deactivated ZrO_2-573 could be readily regenerated *via* simple calcination at 573 K for 4 h. The EL conversion of 77.2% and GVL yield of 58.4% obtained when the regenerated ZrO_2-573 was used in the fifth cycle were parallel to those obtained in the first cycle. The characterization of the spent catalyst was also conducted, and the results are given in the ESI.† Compared with the fresh catalyst, the surface area of the spent catalyst was decreased slightly (Table S2, ESI†). Meanwhile, there was not a noticeable difference between the surface area of the spent catalysts and the regenerated catalyst. However, an obvious drop in EL conversion and GVL yield were observed after the fourth reaction cycle, and the comparable catalytic activity of ZrO_2-573 was recovered after regeneration. The above-mentioned results show that the loss of the activity of spent ZrO_2-573 was largely due to humins deposited on the surface of the ZrO_2-573, the regeneration process removed the humins and recovered the catalytic activity. It is noteworthy that the reactivated ZrO_2-573 catalyst was totally converted to the tetragonal phase from the amorphous phase (Fig. S3, ESI†), although the size of primary crystallites and surface morphology of the catalysts were not changed evidently before and after regeneration (Fig. S4, ESI†).

Poisoning experiments were also carried out by introducing extra additives into the reaction system, and the results are depicted in Fig. 8. In the presence of pyridine, the catalytic activity of ZrO_2-573 was slightly decreased. It is probable that the poor adsorption performance of pyridine on the surface of the catalyst led to the weak poisoning effect.[38] However, the

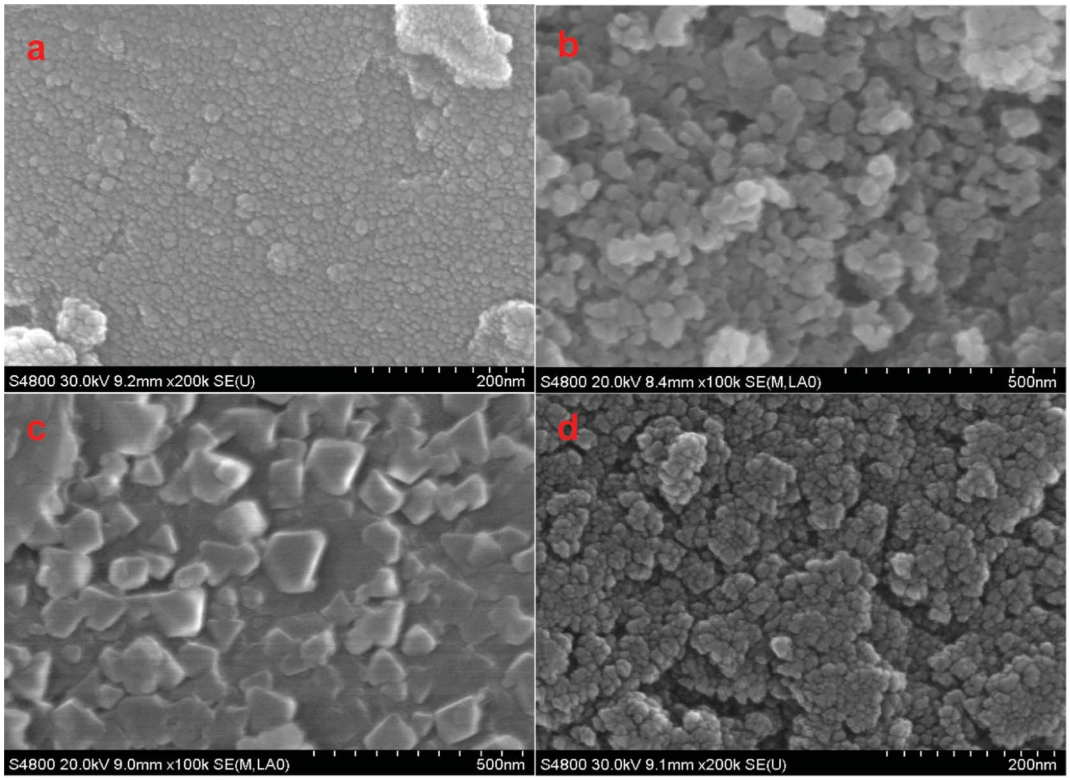

Fig. 5 SEM images for (a) ZrO_2-573, (b) ZrO_2-773, (c) ZrO_2-973 and (d) ZrO_2-573 recovered after cycle 4.

addition of benzoic acid drastically reduced the conversion of EL. This can be explained by the strong interaction between benzoic acid and base sites. Meanwhile, it should be noted that ZrO_2-573 was very sensitive to sulfuric acid and sodium hydroxide. A significant decrease in EL conversion and GVL yield was observed when sulfuric acid or sodium hydroxide was added. Furthermore, the addition of small amounts of water did not substantially change the catalytic activity of ZrO_2-573, 78.4% EL conversion and a 59.8% GVL yield were still obtained.

Table 2 Conversion of EL into GVL under various conditions[a]

Entry	Tem. (K)	Pressure[b] (bar)	GVL yield (%)	EL conversion (%)
1	453	20	23.4	35.9
2	463	24	24.3	38.7
3	473	30	26.4	41.6
4	483	36	52.1	65.2
5	493	42	54.1	66.5
6	503	52	59.0	70.4
7	513	60	61.8	74.0
8	523	70	62.5	81.5
9[c]	523	70	43.0	55.6
10	533	86	60.8	83.7
11[d]	523	70	28.6	32.1
12[e]	523	70	12.7	14.3

[a] Reaction conditions: EL, 2 g; ZrO_2-573 catalyst, 1 g; ethanol, 38 g; reaction time, 1 h. [b] Reaction pressure is obtained by the swelling of ethanol itself at the specified temperature. [c] 4 g EL as feed. [d] ZrO_2-773 as the catalyst. [e] ZrO_2-973 as the catalyst.

The above mentioned poisoning experiments revealed that the process of CTH for the conversion of EL into GVL was closely related to the acid–base property of ZrO_2. Combined with the results of the catalyst characterization, a plausible mechanism of CTH analogous to that presented by Ivanov *et al.*[38] was presented (Scheme 3). Hydrogen transfer is a concerted process that takes place *via* a six-membered ring transition state formed between ethanol and EL. The rate-determining step of the process must be related to the interaction of the alcohol with the acid–base sites (unsaturated Zr^{4+}–O^{2-} pairs), which causes its dissociation to the corresponding alkoxide. The surface-adsorbed alkoxide transfers a hydride ion that attacks the carbonyl group of EL to yield ethyl 4-hydroxypentanoate (4-HPE), and then the 4-HPE is further converted into GVL through an intramolecular transesterification accompanied by the equimolar production of ethanol. Meanwhile, the ethanol is converted into the corresponding acetaldehyde after losing two hydrogens, then the latter condensed with two ethanol molecules to afford acetal. Although acetal was determined as the second product to GVL by a GC-MS analysis, no detectable 4-HPE was observed. This result indicated that the rate of intramolecular transesterification of 4-HPE is very fast under the reaction temperature. In addition, some derivatives of GVL were identified from a GC-MS analysis (Scheme S1, ESI†), but the reaction mechanism involving these derivatives is not very clear.

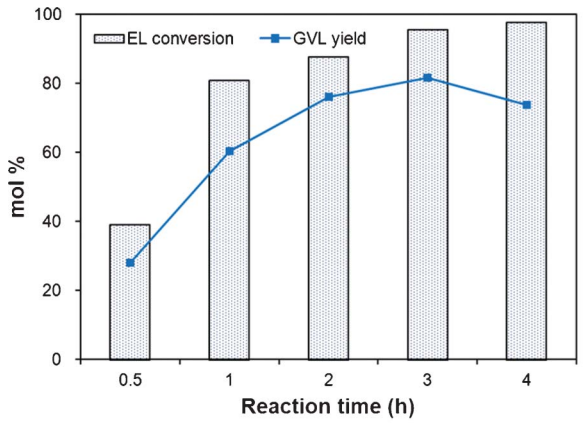

Fig. 6 Effect of reaction time on the conversion of EL into GVL. Reaction conditions: EL, 2 g; ZrO_2-573, 1 g; ethanol, 38 g; reaction temperature, 523 K.

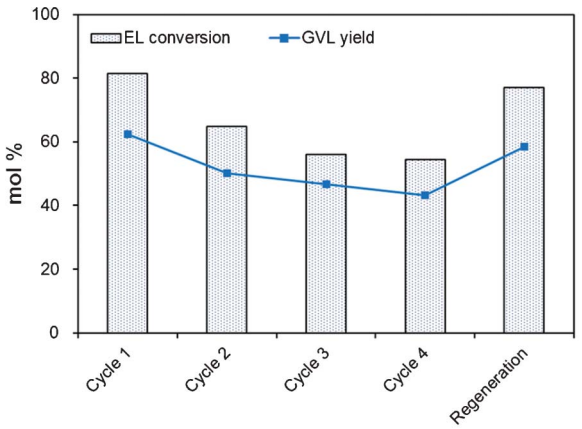

Fig. 7 Recycling of the catalysts in the conversion of EL into GVL. Reaction conditions: EL, 2 g; ZrO_2-573, 1 g; ethanol, 38 g; reaction temperature, 523 K; reaction time, 1 h. Catalyst regeneration: calcination at 573 K for 4 h after cycle 4.

Further understanding of these minor-products is essential and will be the focus of future studies, however this issue is not of primary concern in this paper.

Conclusions

In the present work, a series of ZrO_2 catalysts were prepared, characterized and used for the synthesis of GVL from biomass-derived EL in the presence of supercritical ethanol that could be employed as the hydrogen source and reaction solvent simultaneously. Among various ZrO_2 catalysts, amorphous ZrO_2 was found to be the most active, a yield of GVL and a conversion of EL as high as 81.5 and 95.5% were achieved at 523 K for 3 h, respectively. Fortunately, the ZrO_2-573 regenerated through simple calcination still had excellent stability and reusability after the fifth cycle. Moreover, a mechanism for the conversion of EL into GVL *via* CTH was also proposed according to the results of the catalyst characterization and the poisoning experiments. To the best of our knowledge, this work is the first to report this approach to the synthesis of GVL directly from EL using supercritical ethanol as a the hydrogen donor.

Table 3 Effect of catalyst loading on the conversion of EL into GVL[a]

Entry	Catalyst loading (g)	GVL yield (%)	EL conversion (%)
1	0.0	0.8	1.7
2	0.3	37.7	46.0
3	0.5	46.2	54.6
4	0.8	56.9	71.8
5	1.0	62.5	81.5
6	1.2	62.9	82.3

[a] Reaction conditions: EL, 2 g; catalyst, ZrO_2-573; ethanol, 38 g; reaction temperature, 523 K; reaction time, 1 h.

Experimental procedure

Materials

EL (98%) and GVL (98%) were purchased from Alfa Aesar Co. Ltd. (Tianjin, China). Zirconium oxychloride (99%) was obtained from Aladdin Reagent Co. Ltd. (Shanghai, China). All other chemicals were supplied from Sinopharm Chemical Reagent Co. Ltd. (Shanghai, China) and used without further purification.

Catalysts preparation

$ZrOCl_2 \cdot 8H_2O$ was dissolved in deionized water to prepare a 100 g L^{-1} $ZrOCl_2 \cdot 8H_2O$ solution. Concentrated NH_4OH was added to adjust the pH value to between 9 and 10 with vigorous stirring, and then aged at room temperature for 24 h. The obtained precipitate was thoroughly washed with deionized water until chloride ions could not be identified in the filtrate. The washed precipitate was dried at 383 K for 12 h, and then

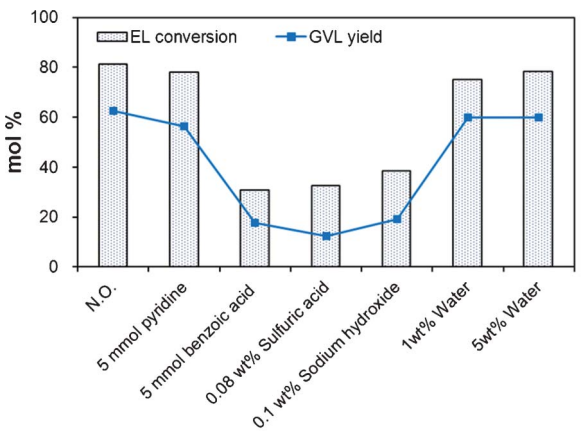

Fig. 8 Effect of extra additives on the conversion of EL into GVL. Reaction conditions: EL, 2 g; ZrO_2-573, 1 g; ethanol, 38 g; reaction temperature, 523 K; reaction time, 1 h. N.O. means that no additives were introduced to the reaction system.

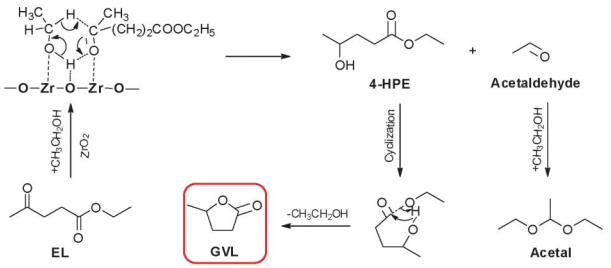

Scheme 3 Proposed mechanism for the conversion of EL into GVL over ZrO_2 in supercritical ethanol *via* CTH.

calcined at 573 K, 773 K and 973 K for 12, 6 and 6 h, respectively. The prepared catalysts were labeled as ZrO_2-573, ZrO_2-773 and ZrO_2-973, respectively.

Catalyst characterization

SEM images were performed on a Hitachi S-4800 by using 20 kV or 30 kV. X-ray diffraction (XRD) patterns were obtained on a Panalytical X'pert Pro diffractometer using a Cu-Kα radiation source with the following parameters: 40 kV, 30 mA, 2θ from 5° to 80° at a scanning speed of 3° min^{-1}. FT-IR spectra were recorded on a Nicolet 330 spectrometer. Thermal gravimetric analysis and differential thermal gravimetric analysis (TGA/DTG) were carried out on a SDT Q600 thermal analyzer under a dynamic N_2 atmosphere (100 mL min^{-1}) in the temperature range of 293–1173 K with a heating rate of 20 K min^{-1}, each sample was held isothermally at 373 K for 30 min before ramping up to 1173 K. BET surface areas were measured on a TriStar 3000 surface area and porosimetry analyzer (Micromeritics), the samples were degassed at 573 K for 3 h in a vacuum before N_2 adsorption. NH_3 temperature-programmed desorption (NH_3-TPD) and CO_2 temperature-programmed desorption (CO_2-TPD) were carried out with a Micromeritics AutoChem II 2920, which was connected to a ThermoStar GSD 301T2 mass spectrometer (Pfeiffer Vacuum). Typically, the sample (200 mg) loaded into the quartz tube was first pretreated at a rate of 15 K min^{-1} up to 573 K in a He gas flow for 1 h to remove species adsorbed on the surface. The adsorption of NH_3 was performed at 373 K in an NH_3–He (10 vol% NH_3) mixture for 1 h, and then the remaining and weakly adsorbed NH_3 was purged with high-purity He. TPD was performed in the He flow by raising the temperature to 873 K at a rate of 15 K min^{-1} and then keeping it at 873 K for 30 min. The desorbed NH_3 was detected by the mass spectrometer. CO_2-TPD was performed by using a similar procedure.

Typical procedure for the production of GVL

The experiments were carried out in a 100 mL cylindrical stainless steel high-pressure reactor made by the PARR instrument company, USA. 2 g EL, 38 g ethanol and 1 g solid catalyst were mixed and heated at 523 K and stirred at 500 rpm for 1 h. At the end of the reaction, the reactor was cooled to room temperature. The liquid products were centrifuged at 10 000 rpm for 5 min and analyzed by means of GC.

GC analysis

GVL and EL in the reaction mixture were analyzed on an Agilent 7890 series equipped with a HP-5 capillary column (30.0 m × 320 μm × 0.25 μm) and a flame ionization detector (FID) operating at 543 K. The carrier gas was N_2 with a flow rate of 1.0 mL min^{-1}. The following programmed temperature was used in the analysis: 313 K (4 min)–15 K min^{-1}–623 K (5 min). The yield of GVL and the conversion of EL were calculated using the following equations:

$$\text{EL conversion } (\%) = \left(1 - \frac{\text{Mole of EL}}{\text{Initial mole of EL}}\right) \times 100\% \quad (1)$$

$$\text{GVL yield } (\%) = \frac{\text{Mole of EL}}{\text{Initial mole of EL}} \times 100\% \quad (2)$$

Acknowledgements

This work was financially supported by the National Basic Research Program of China (2010CB732201), the National Natural Science Foundation of China (21106121), the Provincial R&D Program from Economic and Trade Committee of Fujian Province of China (1270-K42004), the Fundamental Research Funds for the Central Universities (2010121077) and the Fundamental Research Funds for the Xiamen University (201212G006).

References

1 L. Hu, G. Zhao, W. Hao, X. Tang, Y. Sun, L. Lin and S. Liu, *RSC Adv.*, 2012, **2**, 11184.
2 A. Corma, S. Iborra and A. Velty, *Chem. Rev.*, 2007, **107**, 2411.
3 G. W. Huber, S. Iborra and A. Corma, *Chem. Rev.*, 2006, **106**, 4044.
4 E. L. Kunkes, D. A. Simonetti, R. M. West, J. C. Serrano-Ruiz, C. A. Gärtner and J. A. Dumesic, *Science*, 2008, **322**, 417.
5 G. W. Huber, J. N. Chheda, C. J. Barrett and J. A. Dumesic, *Science*, 2005, **308**, 1446.
6 A. J. Ragauskas, C. K. Williams, B. H. Davison, G. Britovsek, J. Cairney, C. A. Eckert, W. J. Frederick Jr., J. P. Hallett, D. J. Leak, C. L. Liotta, J. R. Mielenz, R. Murphy, R. Templer and T. Tschaplinski, *Science*, 2006, **311**, 484.
7 I. T. Horváth, H. Mehdi, V. Fábos, L. Boda and L. T. Mika, *Green Chem.*, 2008, **10**, 238.
8 Y. Zhao, Y. Fu and Q. X. Guo, *Bioresour. Technol.*, 2012, **114**, 740.
9 J. P. Lange, J. Z. Vestering and R. J. Haan, *Chem. Commun.*, 2007, 3488.
10 D. M. Alonso, J. Q. Bond, J. C. Serrano-Ruiz and J. A. Dumesic, *Green Chem.*, 2010, **12**, 992.
11 D. Fegyverneki, L. Orha, G. Láng and I. T. Horváth, *Tetrahedron*, 2010, **66**, 1078.
12 J. Q. Bond, D. M. Alonso, D. Wang, R. M. West and J. A. Dumesic, *Science*, 2010, **327**, 1110.

13 T. J. Bruno, A. Wolk and A. Naydich, *Energy Fuels*, 2010, **24**, 2758.
14 X. L. Du, Q. Y. Bi, Y. M. Liu, Y. Cao, H. Y. He and K. N. Fan, *Green Chem.*, 2012, **14**, 935.
15 J. Q. Bond, D. Wang, D. M. Alonso and J. A. Dumesic, *J. Catal.*, 2011, **281**, 290.
16 K. Yan, J. Liao, X. Wu and X. Xie, *RSC Adv.*, 2013, **3**, 3853.
17 A. M. Raspolli Galletti, C. Antonetti, E. Ribechini, M. P. Colombini, N. Nassi O Di Nasso and E. Bonari, *Appl. Energy*, 2013, **102**, 157.
18 S. G. Wettstein, J. Q. Bond, D. M. Alonso, H. N. Pham, A. K. Datye and J. A. Dumesic, *Appl. Catal. B.*, 2012, **117–118**, 321.
19 R. A. Bourne, J. G. Stevens, J. Ke and M. Poliakoff, *Chem. Commun.*, 2007, 4632.
20 Z. p. Yan, L. Lin and S. Liu, *Energy Fuels*, 2009, **23**, 3853.
21 M. G. Al-Shaal, W. R. H. Wright and R. Palkovits, *Green Chem.*, 2012, **14**, 1260.
22 A. M. Raspolli Galletti, C. Antonetti, V. De Luise and M. Martinelli, *Green Chem.*, 2012, **14**, 688.
23 H. Heeres, R. Handana, D. Chunai, C. B. Rasrendra, B. Girisuta and H. J. Heeres, *Green Chem.*, 2009, **11**, 1247.
24 J. M. Tukacs, D. Király, A. Strádi, G. Novodárszki, Z. Eke, G. Dibó, T. Kégl and L. T. Mika, *Green Chem.*, 2012, **14**, 2057.
25 W. Li, J. H. Xie, H. Lin and Q. L. Zhou, *Green Chem.*, 2012, **14**, 2388.
26 P. P. Upare, J. M. Lee, D. W. Hwang, S. B. Halligudi, Y. K. Hwang and J. S. Chang, *J. Ind. Eng. Chem.*, 2011, **17**, 287.
27 L. Deng, J. Li, D. M. Lai, Y. Fu and Q. X. Guo, *Angew. Chem., Int. Ed.*, 2009, **48**, 6529.
28 L. Deng, Y. Zhao, J. Li, Y. Fu, B. Liao and Q. X. Guo, *ChemSusChem*, 2010, **3**, 1172.
29 X. L. Du, Q. Y. Bi, Y. M. Liu, Y. Cao and K. N. Fan, *ChemSusChem*, 2011, **4**, 1838.
30 X. L. Du, L. He, S. Zhao, Y. M. Liu, Y. Cao, H. Y. He and K. N. Fan, *Angew. Chem., Int. Ed.*, 2011, **50**, 7815.
31 L. C. Peng, L. Lin, H. Li and Q. Yang, *Appl. Energy*, 2011, **88**, 4590.
32 W. J. Xu, W. Zhao, C. Sheng, S. T. Zhong, X. N. Wu, C. H. Yan, S. Bai, Z. M. Zong and X. Y. Wei, *Energy Fuels*, 2010, **24**, 250.
33 M. Chia and J. A. Dumesic, *Chem. Commun.*, 2011, **47**, 12233.
34 E. Djurado, P. Bouvier and G. Lucazeau, *J. Solid State Chem.*, 2000, **149**, 399.
35 K. G. Kanade, J. O. Baeg, S. K. Apte, T. L. Prakash and B. B. Kale, *Mater. Res. Bull.*, 2008, **43**, 723.
36 M. A. Aramendía, V. Borau, C. Jiménez, J. M. Marinas, J. R. Ruiz and F. J. Urbano, *Appl. Catal., A*, 2003, **244**, 207.
37 G. Y. Guo and Y. Chen, *J. Mater. Sci.*, 2004, **39**, 4039.
38 V. A. Ivanov, J. Bachelier, F. Audry and J. C. Lavalley, *J. Mol. Catal.*, 1994, **91**, 45.

